ELSEVIER

Journal of Chromatography A, 810 (1998) 1–17

JOURNAL OF CHROMATOGRAPHY A

Study of the thermodynamics and mass transfer kinetics of two enantiomers on a polymeric imprinted stationary phase

Peter Sajonz[a,b], Marianna Kele[a,b], Guoming Zhong[a,b], Börje Sellergren[c], Georges Guiochon[a,b,*]

[a]*Department of Chemistry, University of Tennessee, Knoxville, TN 37996-1600, USA*
[b]*Division of Chemical and Analytical Sciences, Oak Ridge National Laboratory, Oak Ridge, TN 37831, USA*
[c]*Department of Inorganic Chemistry and Analytical Chemistry, Johannes Gutenberg University, Mainz, Joh.-Joachim-Becherweg 24, D-55099 Mainz, Germany*

Received 24 November 1997; received in revised form 13 March 1998; accepted 13 March 1998

Abstract

The adsorption isotherms of D- and L-phenylalanine anilide (PA) on an L-phenylalanine anilide imprinted stationary phase have been determined using staircase frontal analysis. An aqueous buffer–organic solvent mixture has been used as mobile phase. The measurements were done at temperatures of 40, 50, 60 and 70°C for sample concentrations ranging between $5 \cdot 10^{-4}$ to 1 g/l. It was found that the adsorption data fit well to both the Freundlich and the Bi-Langmuir isotherm models. Examination of the best values of the numerical coefficients of the Bi-Langmuir model shows that the site class representing the binding sites with the highest binding energy exhibits a very low saturation capacity for the non-imprinted enantiomer, indicating a high selectivity for the imprinted L-enantiomer. The low energy site class also shows some selectivity for the L-enantiomer. Mass transfer rate coefficients were obtained for each single breakthrough curve by using the transport model of chromatography. It was found that the mass transfer coefficient of L-PA increases very rapidly with the sample concentration while there is only a slight increase for the other enantiomer.

Keywords: Thermodynamic parameters; Kinetic studies; Mass transfer; Enantiomer separation; Adsorption isotherms; Imprinted polymers; Stationary phases, LC; Phenylalanine anilide

1. Introduction

The technique of molecular imprinting consists of the self-assembly of a functional monomer and a template molecule in solution followed by the co-polymerization of the functional monomer and an excess of an appropriate crosslinking monomer. After dissolution of the small molecule template, the resulting network polymer exhibits a significantly higher affinity for the molecule used as the template than for similar molecules, including closely related isomers [1–6]. For example, polymers imprinted with a pure enantiomer may differentiate between the template and the other enantiomer. Thus, the method is very attractive because it allows the custom design of stationary phases selective for a specific enantiomer, the imprint molecule [6]. The recognition can be explained in terms of functional group and shape complementarity between the template and the architecture of binding sites in the imprinted polymer.

*Corresponding author.

0021-9673/98/$19.00
PII: S0021-9673(98)00247-7

To some extent, it can be predicted. In some cases, affinities and selectivities approaching those observed for biological recognition elements have been obtained.

Although the selectivity is usually high, the imprinted polymers are generally associated with a poor chromatographic efficiency and the elution of broad and asymmetric peaks [7]. Such poor performance is usually attributed to mass overloading and/or to slow mass transfer. The first effect is common with imprinted phases, due to a heterogenous distribution of the binding sites. This phenomenon has been quantified in a number of cases [8–11]. The heterogeneity of the adsorbent has been attributed to two factors: (a) during self-assembly, the monomer–template association is incomplete. A relatively large fraction of the monomer units remain nonassociated and these units are responsible for nonspecific binding. (b) The amorphous nature of the polymer structure results in the nonequivalence of the different binding sites. A situation may then arise in which only a fraction of the added template molecules are incorporated as higher complexes with the functional monomer. These complexes are believed to result in high energy binding sites [12]. Important peak asymmetry could originate from a combination of the overloading of these sites and the slow mass transfer kinetics which is always associated with high energy sites [13].

The importance of mass transfer limitations in molecular imprinting has so far not been quantified. Mass transfer limitations result in peak broadening and asymmetry and may be caused by slow diffusion through a polymer network or by slow interactions at the binding sites. A key to improving the performance of imprinted polymers would thus be either to achieve a narrower site distribution (e.g., by blocking the high or low affinity site classes or using monomers with a higher affinity for the template) or to increase the accessibility of the binding sites. The former requires chemical modifications whereas the latter can be affected by changing the polymer morphology. In order to clearly understand the influence of such modifications a thorough investigation of the thermodynamic and kinetic parameters involved is necessary. Such an investigation involves measuring the adsorption equilibrium isotherms and the mass transfer kinetic parameters [13], data which are missing in the case of imprinted polymers. One powerful technique for the study of the interactions between solutes and stationary phases and for the investigation of the parameters of these interactions is frontal analysis [13–15]. This method allows the accurate determination of adsorption and kinetic data from simple breakthrough experiments. Previous studies have demonstrated the validity of this approach [4–7]. Experimental results have suggested that the mass transfer coefficient was concentration dependent [6–8]. It would be important to validate this concept by collecting similar observation on a variety of stationary phases and solutes.

This work reports on the measurement of the equilibrium isotherms and the mass transfer coefficients of D- and L-phenylalanine anilide (PA) on a polymeric phase imprinted with L-phenylalanine anilide. The results of these measurements will be used in forthcoming publications to investigate the effect of polymer structure and morphology as well as chemical and thermal treatments on the isotherm shape and mass transfer kinetics.

2. Theory

The classical transport model [13] was used in this study. It is a simple model of the chromatographic process. It assumes that there is no axial dispersion in the column and that band broadening is only caused by the resistance to mass transfer. In other words, for the sake of simplicity, we neglect the influence of axial and eddy diffusion compared to that of the mass transfer kinetics. Only a brief description of the model is given below. Details are available in the literature [13].

2.1. Mass balance

The differential mass balance of the transport model for a single component is written

$$\frac{\partial C}{\partial t} + F\frac{\partial q}{\partial t} + u\frac{\partial C}{\partial z} = 0 \quad (1)$$

where C and q are the concentrations of the compound studied in the mobile and the stationary phase, respectively, F is the phase ratio and u the linear velocity of the mobile phase. In the following,

concentrations are expressed in mass of solute per unit volume of liquid phase (C) or of column bed (q). The parameters t and z represent the time and the location in the column, respectively. Reference points for these parameters are the start of an experiment with $t=0$ and the column inlet with $z=0$.

2.2. Mass transfer kinetics

In the transport model, band broadening is accounted for by using the solid film linear driving force model, which lumps all contributions into one mass transfer rate coefficient, k_f, and is expressed by the equation

$$\frac{\partial q}{\partial t} = k_f(q^* - q) \tag{2}$$

where q^* is the concentration in the stationary phase at equilibrium while q is the local solid-phase concentration at time t. Since the axial dispersion coefficient in Eq. (1) is assumed to be nil, Eq. (2) accounts also for axial dispersion and the rate coefficient includes the corresponding contribution. The mass transfer rate coefficient is often considered to be independent on the sample concentration in the mobile phase. However, it has been shown in many cases [14–22] that this is not so. For reasons explained later, the following relationship has been used in this work:

$$k_f(C) = k_{f,0}C^m \tag{3}$$

where $k_{f,0}$ and m are numerical parameters independent of the concentration.

2.3. Equilibrium isotherm

A relationship between q^* and C is needed for the mass balance to be solved. In this work three isotherm models were used, the Langmuir, Bi-Langmuir and Freundlich isotherm models. The respective equations for these three models are written as follows

$$q^*(C) = \frac{a_1 C}{1 + b_1 C} \tag{4a}$$

$$q^*(C) = \frac{a_1 C}{1 + b_1 C} + \frac{a_2 C}{1 + b_2 C} \tag{4b}$$

$$q^*(C) = aC^{1/n} \tag{4c}$$

In these equations a_1, b_1, a_2, b_2, a and n are numerical parameters. The ratios a_1/b_1 and a_2/b_2 represent the saturation capacities of the compound studied on the corresponding adsorption sites of the stationary phase. The Freundlich isotherm does not have a saturation capacity.

2.4. Initial and boundary conditions

The initial and boundary conditions for the experiments correspond to a column operated in the frontal analysis mode. Initially, the column is filled with the mobile phase containing the studied compound at a concentration C_n. At the beginning of the new experiment ($t=0$), a step injection of a solution of the compound at the concentration C_{n+1} is performed. Consistent with the assumption that the contribution of axial diffusion to band broadening is negligible, the following diffusionless boundary condition is used

$$C(z,0) = C_n \tag{5a}$$

$$C(0,t) = C_{n+1} \quad \text{for } t > 0 \tag{5b}$$

$$\frac{\partial C}{\partial z}(L,t) = 0 \tag{5c}$$

2.5. Numerical solutions

The system of Eqs. (1)–(3), (4a)–(4c), (5a)–(5c) states the transport model of chromatography. There are no analytical solutions for this model. Numerical methods are needed in order to solve it [13]. A computer program has been written for this purpose. Numerical solutions obtained with it have been previously discussed [23,24].

3. Experimental

3.1. Liquid chromatography

A Hewlett-Packard 1090 system was used (Palo Alto, CA, USA). This system is equipped with a multi-solvent delivery system, an automatic injector, a column oven, a diode-array detector and a data

acquisition system. The microcomputer of this system also monitors the operations of the equipment which can be programmed to perform a series of breakthrough curves (see later).

3.2. Chemicals

The monomers, methacrylic acid (MAA) (Aldrich, St. Louis, MO, USA) and ethylene glycol dimethacrylate (EDMA) (Fluka, Buchs, Switzerland) and the solvents were purified as previously described [25]. The initiator, azo-bis-isobutyroninile (AIBN), was obtained from Janssen and purified by recrystallisation. D- and L-Phenylalanine anilide (D- and L-PA, M_r 240.31 g/mol) were synthesized as described elsewhere [26] and purified by crystallization from heptane–chloroform.

3.3. Preparation of the stationary phase and packing of the column

The polymer was synthesized following the general imprinting protocol shown in Fig. 1. L-PA (2 g, 8.3 mmol), MAA (3.4 ml, 0.04 mol), EDMA (38 ml, 0.2 mol) and AIBN (0.4 g, 2.5 mmol) were dissolved in methylene chloride (56 ml). The solution was sparged with nitrogen for about 5 min and transferred into six thick-walled glass polymerization tubes in which it was again sparged with nitrogen. The tubes were then sealed with parafilm, immersed into a water bath maintained at 15°C, allowed to equilibrate for 10 min, and irradiated by a medium pressure Hg lamp (Original Hanau 800) for 24 h. During that time, they were rotated periodically to ensure an even polymerization. Following the end of the polymerization, the polymer monolith was grounded in water in a mechanical ball mill. The procedure was optimized so as to obtain the maximum yield of the required size fraction, 25–35 μm. This fraction was sieved and washed thoroughly with water. A 100×4.6 mm stainless steel HPLC column was packed with a slurry made with ca. 1 g dry weight of packing material and the appropriate volume of a solution of acetonitrile–water–acetic acid (92.5:2.5:5, v/v/v). A primary evaluation of the polymer selectivity was done using an organic mobile phase, MeCN–water–HOAc (92.5:2.5:5, v/v/v), as the mobile phase. Thereafter, the polymers

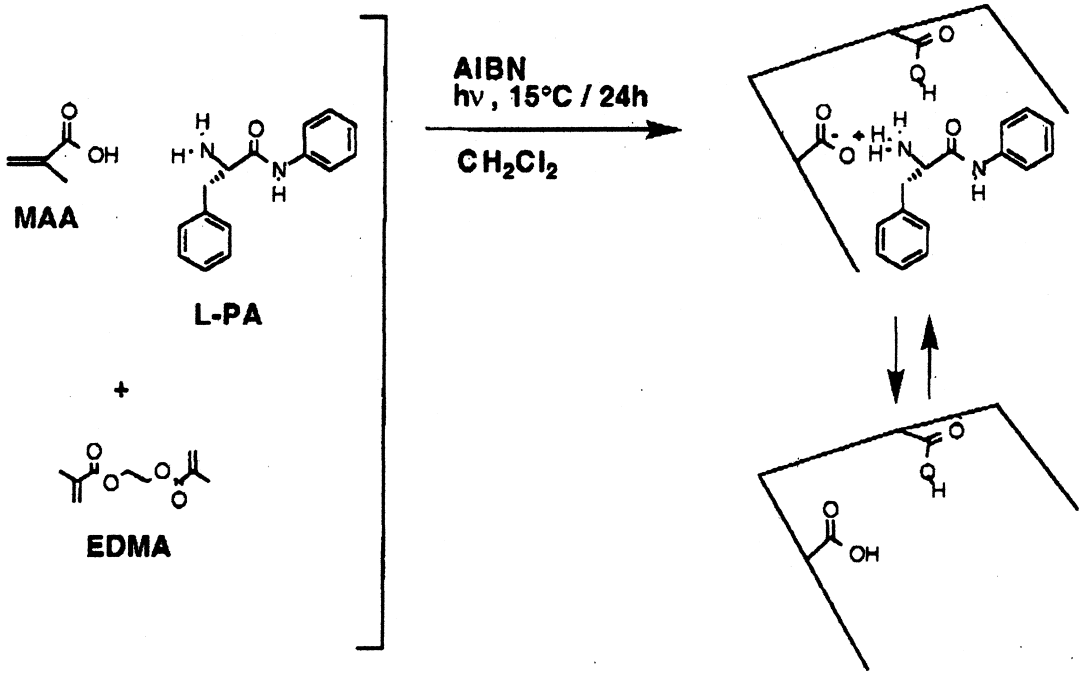

Fig. 1. General imprinting protocol.

were evaluated using an aqueous mobile phase of MeCN–0.05 *M* potassium phosphate (KP) (7:3, v/v) at various pH values.

3.4. Mobile phase and samples

The mobile phase was prepared by dissolving the proper amounts of orthophosphoric acid (Fluka, No. 79622) and sodium hydroxide (Mallinckrodt, No. 7708) into HPLC-grade water (J.T. Baker, No 7732-18-5). The pH was monitored using a calibrated pH meter (American pH II) and adjusted by adding additional amounts of phosphoric acid or sodium hydroxide until the desired pH value was reached, at pH 5.85. The calibration of the pH meter was done by using three pH standard solutions at pH = 4.0, 7.0 and 9.0 (Baxter Diagnostics, CAS No. 7732-18-5, 7778-77-0, 7447-40-7). A mixture of acetonitrile (J.T. Baker, No. 75-05-8)–buffer solution (70:30, v/v) was prepared and used as eluent and for the preparation of the sample solutions required by frontal analysis. Three sample concentrations were prepared for each enantiomer, at 1, 0.1 and 0.01 g/l. All solutions were filtered through 0.45-μm Nylon Filters (Nalgene Filterware NYL 150-0045, Nalgene, NY, USA).

3.5. Determination of adsorption isotherms and mass transfer coefficients

3.5.1. Experimental measurement of breakthrough curves

The two pumps of the HP1090 solvent delivery system were used to perform the series of concentration steps necessary in frontal analysis. The pure mobile phase is placed in the ''weak'' solvent tank and the most concentrated solution of the compound studied which will be used in a series of frontal analysis experiments is placed in the strong solvent tank. The solvent delivery system is programmed to deliver, under constant total flow-rate, at set time intervals, a series of step gradients. Seven successive upward steps were performed, going from 0 to 5%, 5 to 10%, 10 to 20%, 20 to 40%, 40 to 60%, 60 to 80%, and 80 to 100% of strong solvent in the complement of weak solvent, followed by one single downward step, from 100 to 0%. This produces a classical concentration staircase. This experiment can be repeated in a different concentration range for the strong solvent, after washing the column and equilibrating it for at least 30 min. The concentrations of anilide used for the ''strong'' solvent were 1, 0.1 and 0.01 g/l. Finally, the same measurements were carried out at four different temperatures (40, 50, 60 and 70°C), all at a flow-rate of 1 ml/min. The UV detector was calibrated at two different wavelengths, 260 and 280 nm. The use of these two wavelengths made possible the collection of data in the wide concentration range scanned ($5 \cdot 10^{-4}$ to 1 mg/ml). The sampling rate used was 320 ms per data point. The advantage of this procedure is in supplying highly reliable data.

3.5.2. Measurement of the hold-up and the extra column times

The hold-up time was measured by injecting small amounts of pure acetonitrile into the column. A value of $t_0 = 1.019$ min (corrected for the extracolumn volume) at a flow-rate of 1 ml/min was obtained. The phase ratio (volume of stationary phase divided by volume of mobile phase) was calculated from t_0, the volumetric flow-rate and the geometrical volume of the column. The value obtained was $F = 0.631$. The extra column time accounts for the migration of the step front through the tubings between the pump and the column inlet. It was measured by injecting small amounts of acetonitrile and connecting a low dead volume union instead of the column, hence connecting the injector directly to the detector, using the same connection capillaries as for connecting the column. A value of $t_x = 0.611$ min was obtained. The experimental data have been corrected by subtracting t_x.

3.5.3. Calibration of breakthrough curves

The experimental data were calibrated from the absorbance values measured for the plateaus of each staircase experiment, in order to transform detector absorbance units into actual concentration units. A second-order polynomial proved to be suitable as calibration function for all experimental data.

3.5.4. Calculation of isotherm data points

The amount of compound accumulated on the stationary phase (i.e., the amount adsorbed) for each

successive step was calculated using the integral mass balance equation

$$q^*_{n+1} - q^*_n = \frac{(C_{n+1} - C_n)}{F} \cdot \frac{(t_{R,n+1} - t_0)}{t_0} \quad (6)$$

where $t_{R,n+1}$ is the retention time of the $(n+1)$th breakthrough curve. This time is obtained from the half height method, i.e., the center of mass of the concentration step. Previous work has shown that the half height method gives sufficiently accurate results in the present case [24]. The parameter t_0 is the hold-up time of the column, hence the time an inert sample needs to travel through the column.

3.5.5. Fitting of isotherm data to isotherm models

The isotherm data were fitted to three models, the Freundlich, Bi-Langmuir and Langmuir models. A nonlinear regression was applied using a Gauss–Newton algorithm with the Levenberg modification (PCNONLIN 4.2). The following function is minimized in order to obtain the best coefficients for the isotherm parameters

$$\sigma^2 = \sum_{i=1}^{N_D} \frac{(q_i^{*,exp} - q_i^{*,th})^2}{q_i^{*,th}} \quad (7)$$

where N_D is the number of data points and $q_i^{*,exp}$ and $q_i^{*,th}$ are the experimental data points and the points corresponding to the model, respectively. The use of this method forces the calculation to account well for the data in the low concentration range. Hence a better value for the initial slope of the isotherm is obtained. This is necessary because the concentration range investigated is very large.

3.5.6. Determination of mass transfer coefficients

A Fortran computer program was used to calculate the band profiles for the breakthrough curves. The calculated breakthrough curves were fitted to the experimental breakthrough curves by adjusting the value of the rate coefficient k_f which was, at this stage, considered to be constant for each single breakthrough curve. Small adjustments of the retention time of the experimental curves had to be made in some cases in order to bring its mass center at the center of the calculated curve. These adjustments were only a few percent for the experimental data. The rate coefficients obtained represent the value corresponding to the average concentration of each single step.

4. Results and discussion

The experimental isotherms are shown in Fig. 2a (L-PA) and Fig. 2b (D-PA) for the two enantiomers of phenylalanine anilide (symbols: experimental data). Because of the width of the range investigated, both solid- and liquid-phase concentrations are plotted in logarithmic scale. The lines in the main figure illustrate the best fits of the experimental data to the Bi-Langmuir isotherm equation (Eq. (4b)) at 40, 50, 60 and 70°C. The top-left inset shows their best fits to the Langmuir isotherm equation (Eq. (4a)) and the bottom-right inset to the Freundlich isotherm equation (Eq. (4c)). The isotherms obtained by fitting the data to the Langmuir equation is of a quality inferior to the other two. The fittings of the data to the Freundlich and to the Bi-Langmuir equations are both good. A comparison of the residuals listed in Table 1 reveals that the different isotherms of D-PA are best fitted to a Bi-Langmuir model while the isotherms for L-PA are slightly better fitted to a Freundlich isotherm model, particularly at low temperatures. However, at concentrations higher than $4 \cdot 10^{-3}$ g/l (17 μM) in the mobile phase the isotherm data of L-PA are equally well fitted to the Freundlich and to the Bi-Langmuir isotherm models, suggesting the existence of binding sites with higher binding energies $K > 200$ ml/mg (50 000 M^{-1}). Table 2 shows the best values of the isotherm parameters (which are those used for the curves in Fig. 2a and Fig. 2b). Some important conclusions can be drawn from the best coefficients of the Bi-Langmuir fit. First, the binding constants and the saturation capacities agree well with values previously determined [27]. At 40°C for L-PA, these are respectively, 0.35 ml/mg (84 M^{-1}) and ca. 16.1 mg/ml (67 mM) for the class 1 sites and 65.3 ml/mg (16 000 M^{-1}) and 0.17 mg/ml (0.7 mM) for the class 2 sites. For D-PA the respective values are 0.20 ml/mg (48 M^{-1}) and 23.0 mg/ml (96 mM) for the class 1 sites and 22.7 ml/mg (5500 M^{-1}) and 0.07 ml/mg (0.3 mM) for the class 2 sites. Secondly, in view of the small saturation capacities observed for D-PA on these sites, with the exception of the result

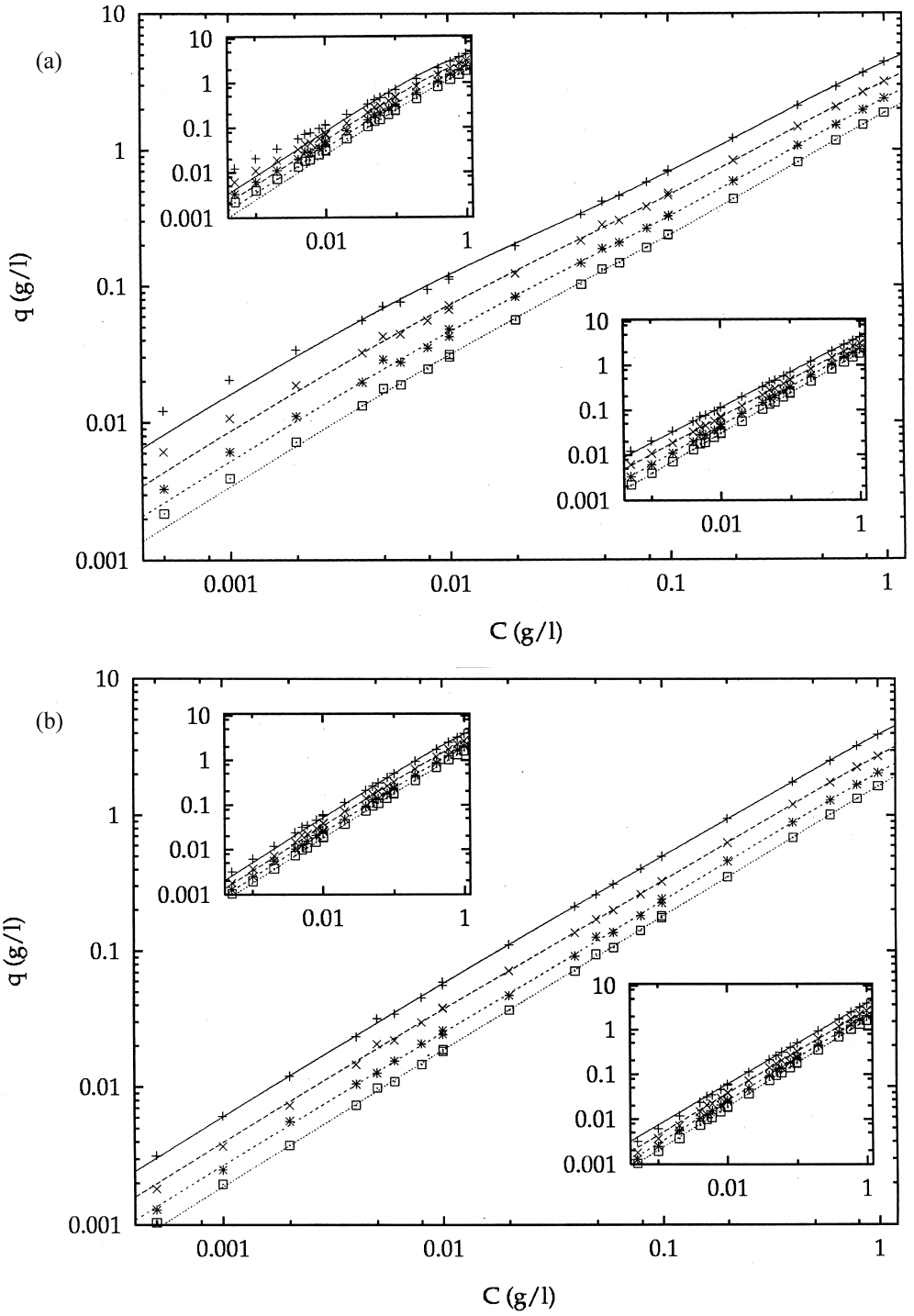

Fig. 2. Experimental isotherm data (symbols) and fittings (lines) to the Bi-Langmuir model (main figure), the Langmuir model (left inset) and the Freundlich model (right inset). 40°C (Solid lines and plus symbols), 50°C (long dashed lines and crosses), 60°C (short dashed lines and stars), 70°C (dotted lines and squares). (a) Solute, L-PA; (b) solute, D-PA.

Table 1
Sum of squared and weighted squared residuals for three isotherm models

Sample	T (°C)	Langmuir	Bi-Langmuir	Freundlich
L-PA	40	0.207927	0.005633	0.000938
		0.237076	0.008723	0.002257
	50	0.071071	0.001975	0.000811
		0.100984	0.005370	0.002554
	60	0.026977	0.000405	0.000464
		0.049659	0.002452	0.001965
	70	0.009776	0.000181	0.000231
		0.021925	0.001007	0.000654
D-PA	40	0.010788	0.000162	0.006307
		0.010990	0.000398	0.004600
	50	0.001995	0.000029	0.002598
		0.004755	0.000343	0.002179
	60	0.000653	0.000352	0.001363
		0.002700	0.001806	0.002963
	70	0.000275	0.000114	0.000246
		0.000874	0.000526	0.000840

obtained at 40°C, the second site class appears to be nearly specific for L-PA. Finally, in agreement with previous findings, the class 1 sites do exhibit a certain selectivity for L-PA.

The determination of the rate coefficients was done by parameter identification, searching for the best value of the rate coefficient which minimizes the difference between each of the experimental breakthrough curves and the curve calculated with the transport model, as explained earlier. An example of this determination is given in Fig. 3, which shows a breakthrough curve of L-PA for a concentration step from 0.01 to 0.02 g/l (symbols, experimental data). The figure shows that the experimental data fits properly to either one of the two isotherm models used (the fit to the Langmuir model, not shown, is poor). The numerical calculation of the breakthrough curve performed with the Bi-Langmuir model (solid lines) gives nearly the same result as the calculation made with the Freundlich isotherm (dashed lines). Three sets of lines are shown, one corresponding to a low rate coefficient of 10 min^{-1}, one to the value of this coefficient which fits best the experimental data ($k_f = 40$ min^{-1}), and one for a high value of 110 min^{-1}. Note, however, that the experimental breakthrough curve is markedly less symmetrical than either of the calculated ones. This suggests strongly a model error, the actual kinetics being much more complex than the one involved in the simple transport model.

The best value of the rate coefficient at 40°C was plotted versus the logarithm of the concentration in Fig. 4. The plot in the main figure is for the rate coefficients obtained using the Bi-Langmuir isotherm

Table 2
Isotherm parameters and standard errors

Sample	T (°C)	Langmuir	Bi-Langmuir		Freundlich
		a_1 b_1 (l/g)	a_1 b_1 (l/g)	a_2 b_2 (l/g)	a (g/l) n
L-PA	40	8.31±0.48	5.62±0.21	10.9±0.9	4.367±0.014
		1.03±0.16	0.35±0.05	65.3±13.5	1.265±0.003
	50	5.27±0.24	3.75±0.14	5.02±0.41	3.162±0.013
		0.75±0.11	0.24±0.05	41.4±9.2	1.209±0.004
	60	3.53±0.13	2.63±0.08	2.69±0.19	2.369±0.010
		0.55±0.08	0.15±0.03	31.5±6.4	1.163±0.004
	70	2.49±0.07	1.99±0.05	1.46±0.09	1.850±0.005
		0.39±0.05	0.11±0.02	28.6±5.5	1.121±0.002
D-PA	40	5.17±0.07	4.60±0.05	1.50±0.07	3.975±0.020
		0.34±0.03	0.20±0.01	22.7±3.8	1.101±0.004
	50	3.37±0.04	3.15±0.03	0.82±0.07	2.776±0.012
		0.25±0.02	0.16±0.01	40.2±10.4	1.074±0.004
	60	2.38±0.02	2.33±0.04	0.40±0.28	2.075±0.012
		0.17±0.02	0.14±0.02	109±176	1.051±0.005
	70	1.81±0.01	1.73±0.05	0.16±0.05	1.647±0.006
		0.11±0.01	0.07±0.03	10.1±11.3	1.034±0.003

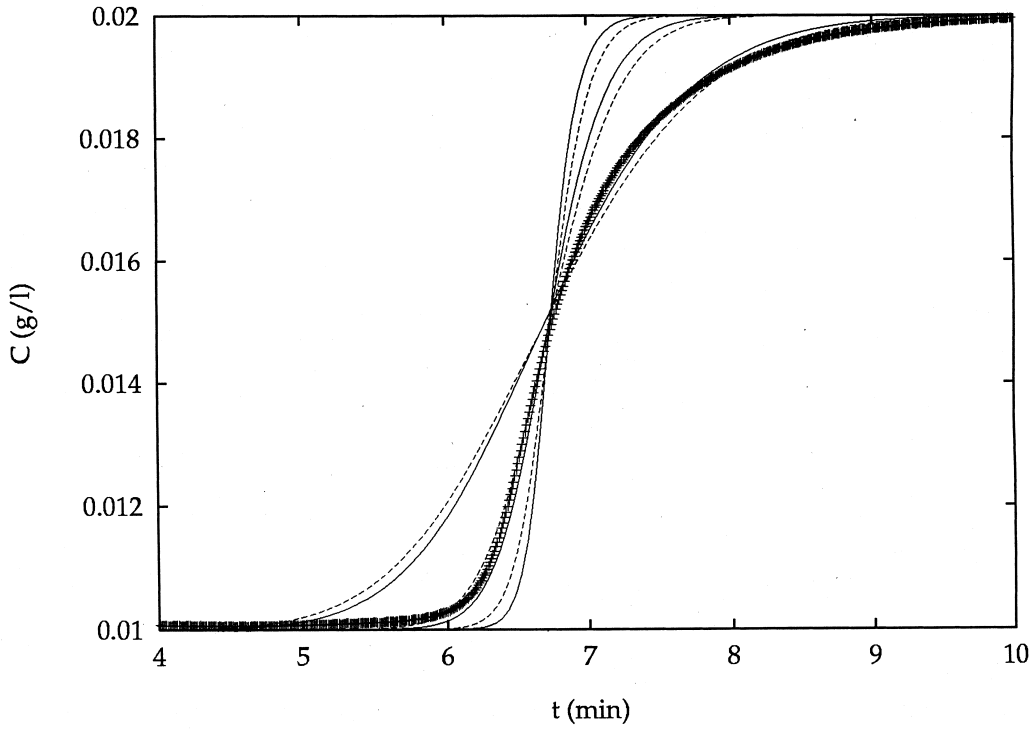

Fig. 3. Example of experimental breakthrough curve (symbols) and fitted curves (lines). The concentration step shown is from $C_n = 0.01$ to $C_{n+1} = 0.02$ g/l. Calculated breakthrough curves for $k_f = 10$ min^{-1}, $k_f = 110$ min^{-1} and for the rate coefficient which fits best the experimental data, $k_f = 40$ min^{-1} (the larger k_f, the steeper the curve). Solid lines: Bi-Langmuir model. Dashed lines: Freundlich model. Sample: L-PA. Temperature: 40°C. The isotherm parameters are listed in Table 2.

model; the plot in the inset is for the rate coefficients obtained with the Freundlich isotherm model. Practically the same values of the rate coefficients were obtained in both cases. This confirms the earlier statement, that both isotherm models fit well the experimental data. For the purpose of the determination of the band broadening data, the isotherm model serves only as a mathematical equation. The facts that the Freundlich isotherm is thermodynamically inconsistent, that the initial slope of the isotherm is infinite and that there is no saturation capacity do not seem to matter much in this instance. Since, at this stage, we are merely looking for an empirical model of our isotherm data, we are justified in using solely the Bi-Langmuir equation for further investigation of the mass transfer kinetics in this work.

Finally, Fig. 4 illustrates the concentration dependence of the rate coefficients for both enantiomers. The lines in this figure show the best fit of the experimental mass transfer rate coefficients to Eq. (3). Although this equation has only two parameters, the fit is quite good. Fig. 5a and Fig. 5b show the results obtained when fitting the values of the rate coefficients obtained at all four temperatures studied to Eq. (3), for the L-enantiomer (Fig. 5a) and the D-enantiomer (Fig. 5b). The concentration dependence is much stronger for the L- than for the D-enantiomer. The values obtained for the rate coefficients of the two enantiomers are listed in Tables 3 and 4. The coefficients of the best fits of these data to Eq. (3) are given in Table 5. At low concentrations the rate coefficients increase with increasing temperature, both for L- and D-PA. At high concentrations the data are too scattered and do not allow a clear conclusion.

Fig. 6a–c (L-PA) and Fig. 7a–c (D-PA) demonstrate the importance of the concentration dependence of the rate coefficient and illustrate the precision of the fitting procedure. The symbols in both

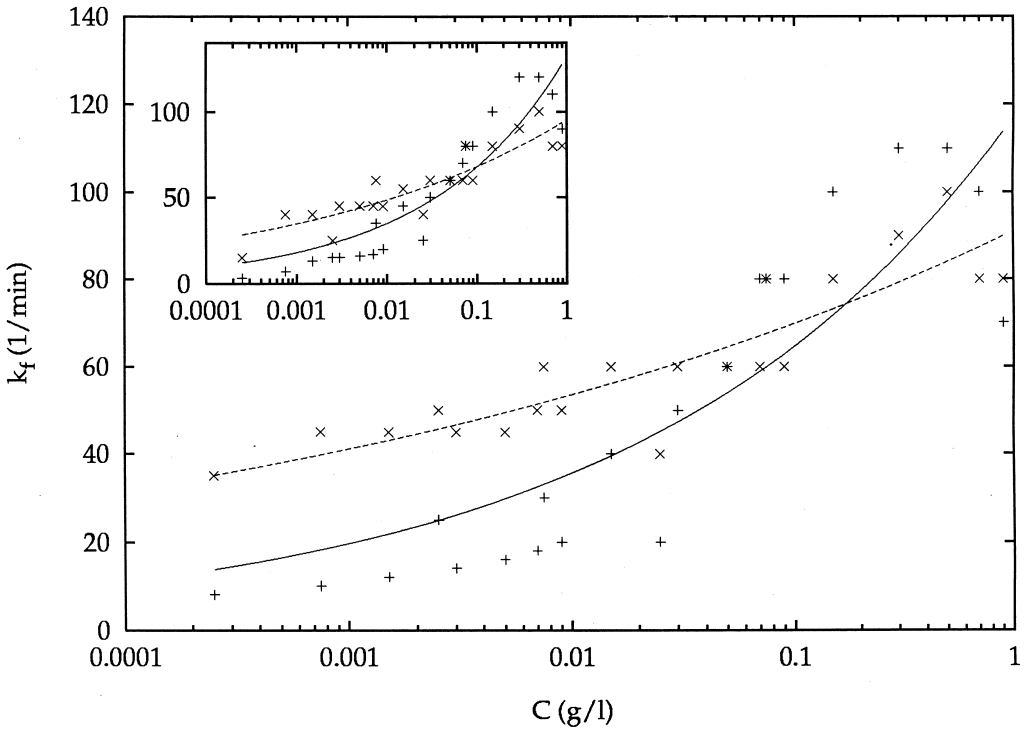

Fig. 4. Comparison of the concentration dependence of k_f obtained for L- and D-PA at 40°C by using two different isotherm models. Bi-Langmuir isotherm (main figure) Freundlich isotherm (inset). Experimental data (symbols) and fittings (lines) to the function $k_f = k_{f,0} C^m$. The best values of the coefficients $k_{f,0}$ and m are listed in Table 5. L-PA: Solid lines and plus symbols. D-PA: Dashed lines and crosses. Star symbols are overlaps of crosses and plus symbols.

figures show the experimental data. The three lines show the results of three sets of numerical calculations, made using two constant values of the rate coefficient, k_f, 10 and 110 min^{-1} (dashed and solid lines, respectively) and using the rate coefficient function of the sample concentration according to Eq. (3). For the sake of convenience, the normalized concentration is plotted versus the time. The concentration steps are 0.0005 to 0.001 g/l in Fig. 6a; they are 10-times and 100-times higher in Fig. 6b and Fig. 6c, respectively. In Fig. 6a, the breakthrough curve calculated with the lower value of k_f (dashed line) fits the experimental data much better than the one calculated using a high value of k_f (solid line). The converse is true for Fig. 6c, in which the breakthrough curve calculated with the high value of k_f gives a better fit than the one derived from the low value of k_f. In Fig. 6b, neither the breakthrough curve calculated with the high value of k_f nor the one derived from the low value results in a good fit. By contrast, the profiles calculated when using Eq. (3) and the best coefficients (Table 4) give reasonably good or better fits in all cases. A similar situation is illustrated in Fig. 7a–c for the D-enantiomer. The concentration dependence is also clearly visible in this case, although it is not as pronounced as for the L-enantiomer. In general, the fits obtained are not as good as those obtained in some other studies [14,15]. The main reason for the differences observed is probably, as indicated earlier, that the mass transfer kinetics are more complex than predicted by the solid film linear driving force model, a result which is not entirely surprising [13,28].

Fig. 8 demonstrates further that, because of the very existence of a concentration dependence of the mass transfer rate coefficient, a fixed value of k_f cannot result in a calculated breakthrough curve that is in good overall agreement with the experimental band profile (symbols), over the whole concentration range, when a large concentration range is spanned

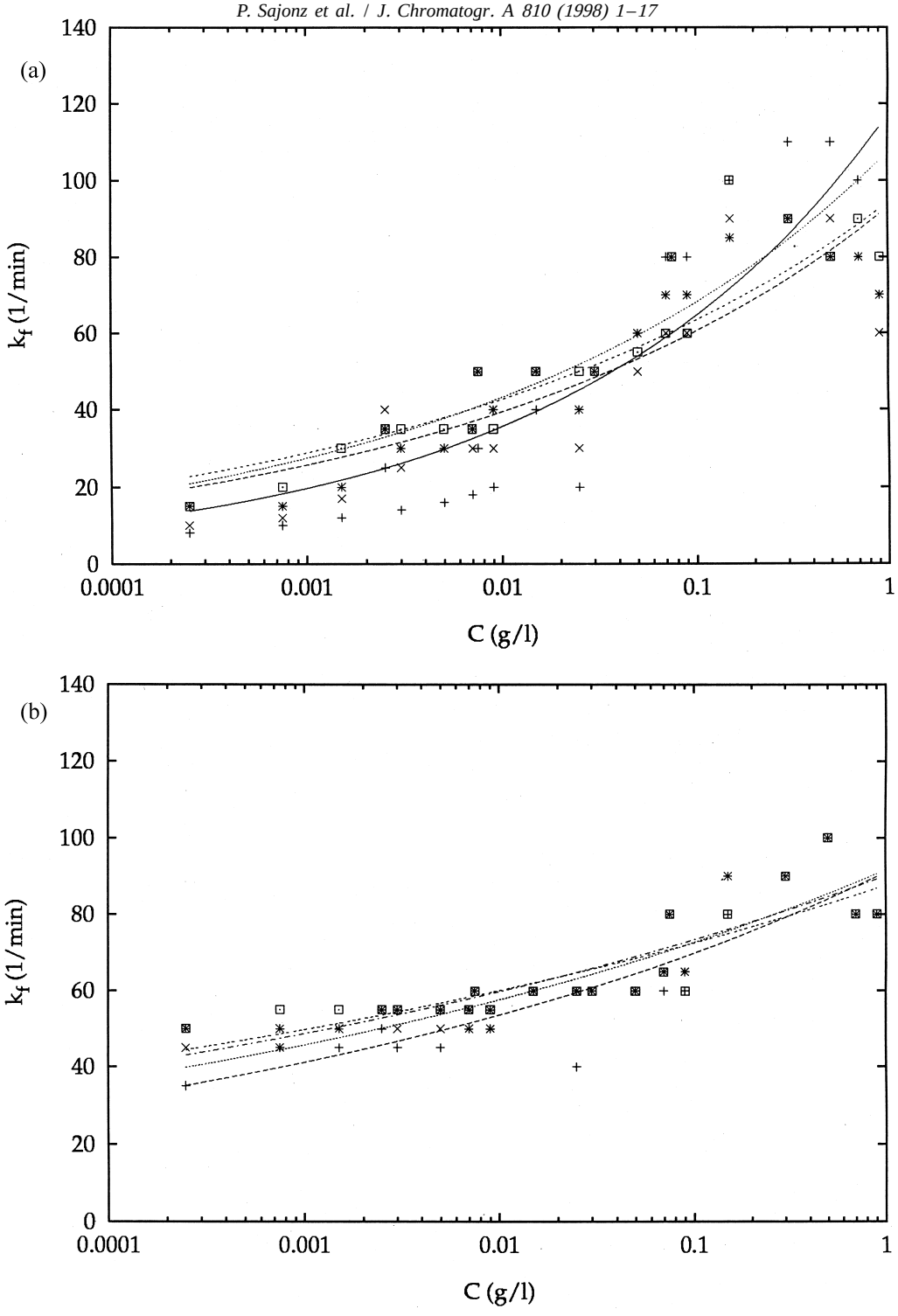

Fig. 5. Experimentally obtained concentration dependence of PA for different temperatures (symbols) and best fit to the function $k_f = k_{f,0} C^m$ (lines). Temperatures: 40°C (plus symbols and solid line), 50°C (crosses and long dashed line), 60°C (stars and dotted line), 70°C (squares and short dashed line). (a) Solute, L-PA; (b) solute, D-PA.

Table 3
Mass transfer rate constants k_f for L-PA

Concentration step (g/l)		Mass transfer rate constant (min^{-1})			
C_n	C_{n+1}	$T=40°C$	$T=50°C$	$T=60°C$	$T=70°C$
0.0	0.0005	8	10	15	15
0.0005	0.001	10	12	15	20
0.001	0.002	13	17	20	30
0.002	0.004	15	25	30	30
0.004	0.006	17	30	30	35
0.006	0.008	19	30	35	35
0.008	0.01	20	30	40	35
0.0	0.005	25	40	35	35
0.005	0.01	30	50	50	50
0.01	0.02	40	50	50	50
0.02	0.04	50	50	50	50
0.04	0.06	60	50	60	55
0.06	0.08	70	60	70	60
0.08	0.1	80	60	70	60
0.0	0.05	20	30	40	50
0.05	0.1	80	70	80	80
0.1	0.2	100	90	85	100
0.2	0.4	110	90	90	90
0.4	0.6	110	90	90	80
0.6	0.8	100	80	80	90
0.8	1.0	70	60	70	80

Table 4
Mass transfer rate constants k_f for D-PA

Concentration step (g/l)		Mass transfer rate constant (min^{-1})			
C_n	C_{n+1}	$T=40°C$	$T=50°C$	$T=60°C$	$T=70°C$
0.0	0.0005	35	45	50	50
0.0005	0.001	45	45	50	55
0.001	0.002	45	50	50	55
0.002	0.004	45	50	55	55
0.004	0.006	45	50	55	55
0.006	0.008	50	50	55	55
0.008	0.01	50	50	55	55
0.0	0.005	50	55	55	55
0.005	0.01	60	60	60	60
0.01	0.02	60	60	60	60
0.02	0.04	60	60	60	60
0.04	0.06	60	60	60	60
0.06	0.08	60	65	65	60
0.08	0.1	60	65	65	60
0.0	0.05	40	60	60	60
0.05	0.1	80	80	80	80
0.1	0.2	80	90	90	90
0.2	0.4	90	90	90	90
0.4	0.6	100	100	100	100
0.6	0.8	80	80	80	80
0.8	1.0	80	80	80	80

Table 5
Best coefficients and standard errors for the concentration dependence of L- and D-PA

Sample	T (°C)	$k_{f,0}$ (min^{-1})	m
L-PA	40	117.3±11.4	0.2582±0.041
	50	92.9±8.0	0.1860±0.030
	60	94.1±6.2	0.1714±0.022
	70	107.2±13.1	0.1971±0.038
D-PA	40	90.9±5.4	0.1147±0.018
	50	91.5±3.9	0.1004±0.012
	60	90.0±3.8	0.0889±0.011
	70	87.5±3.7	0.0817±0.011

The function used was $k_f = k_{f,0} C^m$.

(e.g., in FACP). If it is large, a fixed value of k_f gives a calculated breakthrough curve which fits the experimental curve well in the upper part, at high concentrations. If it is small, a fixed value of k_f results in a calculated breakthrough curve which fits well the low concentration range of the experimental curve only. Fig. 8a illustrates this phenomenon for the L-enantiomer and Fig. 8b for the D-enantiomer. The use of a concentration dependent rate constant, however, did not significantly improve the quality of the fit for the large concentration steps shown. This is probably due to the fact that a backward concentration step does not lead to a shelf sharpening breakthrough curve if the isotherm is convex upwards. The difference between the curves calculated using the high concentration value of the rate coefficient or the concentration-dependent value is small in the low concentration range. It is visible only in the inset which shows a magnification of the low concentration part of the profiles.

Finally, Fig. 9a (L-PA) and Fig. 9b (D-PA) show overloaded elution profiles obtained for three different injection volumes of solutions of the same concentrations of the two enantiomers (dashed lines). The solid lines in these figures show the band profiles numerically calculated for a concentration dependent mass transfer coefficient k_f (main figure), a low-concentration value of k_f (upper inset) and a high-concentration value of k_f (lower inset). For the L-enantiomer, the best fit of the data is obtained using the concentration dependent rate constant, while for the D-enantiomer, the best fit is obtained using a constant value of k_f equal to 35 min^{-1} (low-concentration value). The agreement between experimental and calculated band profiles is good, except in the case of calculations made with the

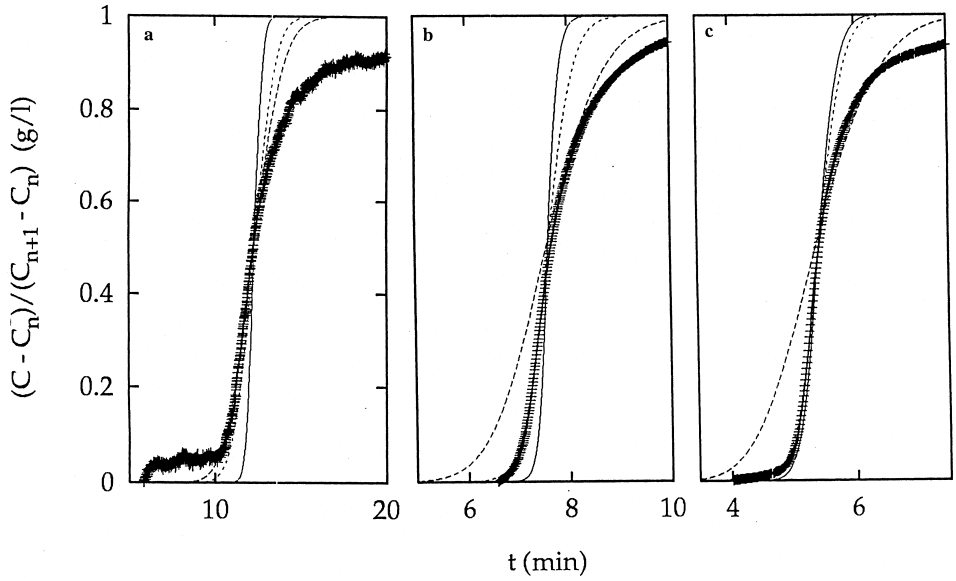

Fig. 6. Comparison between experimental breakthrough curves (symbols) and calculated curves (lines) for L-PA at 40°C. Symbols: experimental data. Long dashed lines: $k_f = 10$ min^{-1}. Solid lines: $k_f = 110$ min^{-1}. Dotted lines: $k_f = 117.3C^{0.2582}$ min^{-1}. (a) $C_n = 0.0005$ g/l, $C_{n+1} = 0.001$ g/l. (b) $C_n = 0.005$ g/l, $C_{n+1} = 0.01$ g/l. (c) $C_n = 0.05$ g/l, $C_{n+1} = 0.1$ g/l.

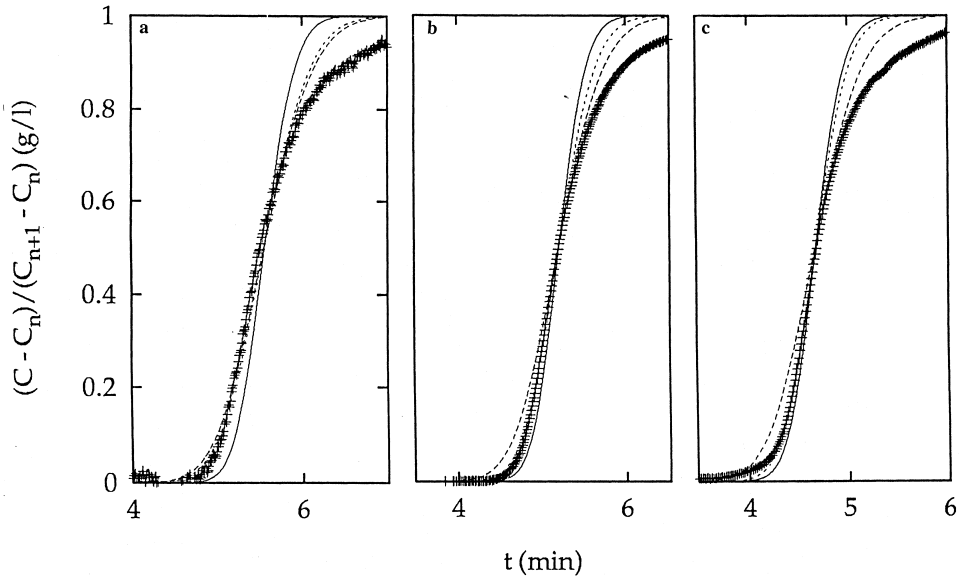

Fig. 7. Comparison between experimental breakthrough curves (symbols) and calculated curves (lines) for D-PA at 40°C. Symbols: experimental data. Long dashed lines: $k_f = 35\ min^{-1}$. Solid lines: $k_f = 90\ min^{-1}$. Dotted lines: $k_f = 90.9C^{0.1147}\ min^{-1}$. (a) $C_n = 0.0005$ g/l, $C_{n+1} = 0.001$ g/l. (b) $C_n = 0.005$ g/l, $C_{n+1} = 0.01$ g/l. (c) $C_n = 0.05$ g/l, $C_{n+1} = 0.1$ g/l.

high-concentration value of the rate coefficient. This is explained by the relatively low average concentrations obtained in elution as compared to the concentration in breakthrough curves.

5. Conclusions

This work shows the importance of a proper handling of the contribution of the mass transfer resistances to band broadening and of the importance of recognizing the dependence of this contribution on the solute concentration. The traditional way of predicting band profiles by measuring the adsorption isotherms in a wide concentration range and the column efficiency in the linear range can lead to faulty conclusions when mass transfer resistances are significant. This is because the implicit assumption of a constant mass transfer rate coefficient is made in this procedure. However, there is now quite a solid body of experimental evidence available that this assumption is often not valid [14–22]. The lower rate constant for L-PA in the low concentration range probably reflects particular mass transfer limitations associated with the high energy sites covered in this concentration range. This phenomenon can be explained by poor site accessibility, if diffusion is the limiting factor, or by a slow interaction with the binding site.

The fact that an excellent fit of the experimental isotherm data is obtained with either a Bi-Langmuir or a Freundlich isotherm is important. The adsorption energy distributions corresponding to these two isotherm models are, respectively, two rays (or in practice, two narrow, well resolved bands) and an exponential decay [29]. The fact that the best value of the exponent of the Freundlich isotherm is close to 1 suggests that the exponential decay constant of the adsorption energy distribution is relatively important. Clearly, the isotherm data of L-PA fit better to the Freundlich isotherm at lower concentrations. This agrees with the isotherm data obtained for some other template polymers that were best fitted to tri-Langmuir models [9–11]. Competitive assays using radiolabeled substrates allowed the identification of a class of sites with a very low surface coverage (ca. 0.2 mg/ml or 1 nmol/ml) and high binding constants, up to $4 \cdot 10^6$ ml/mg ($1 \cdot 10^9\ M^{-1}$). In order to improve the separation performance of imprinted materials to a level compatible with their

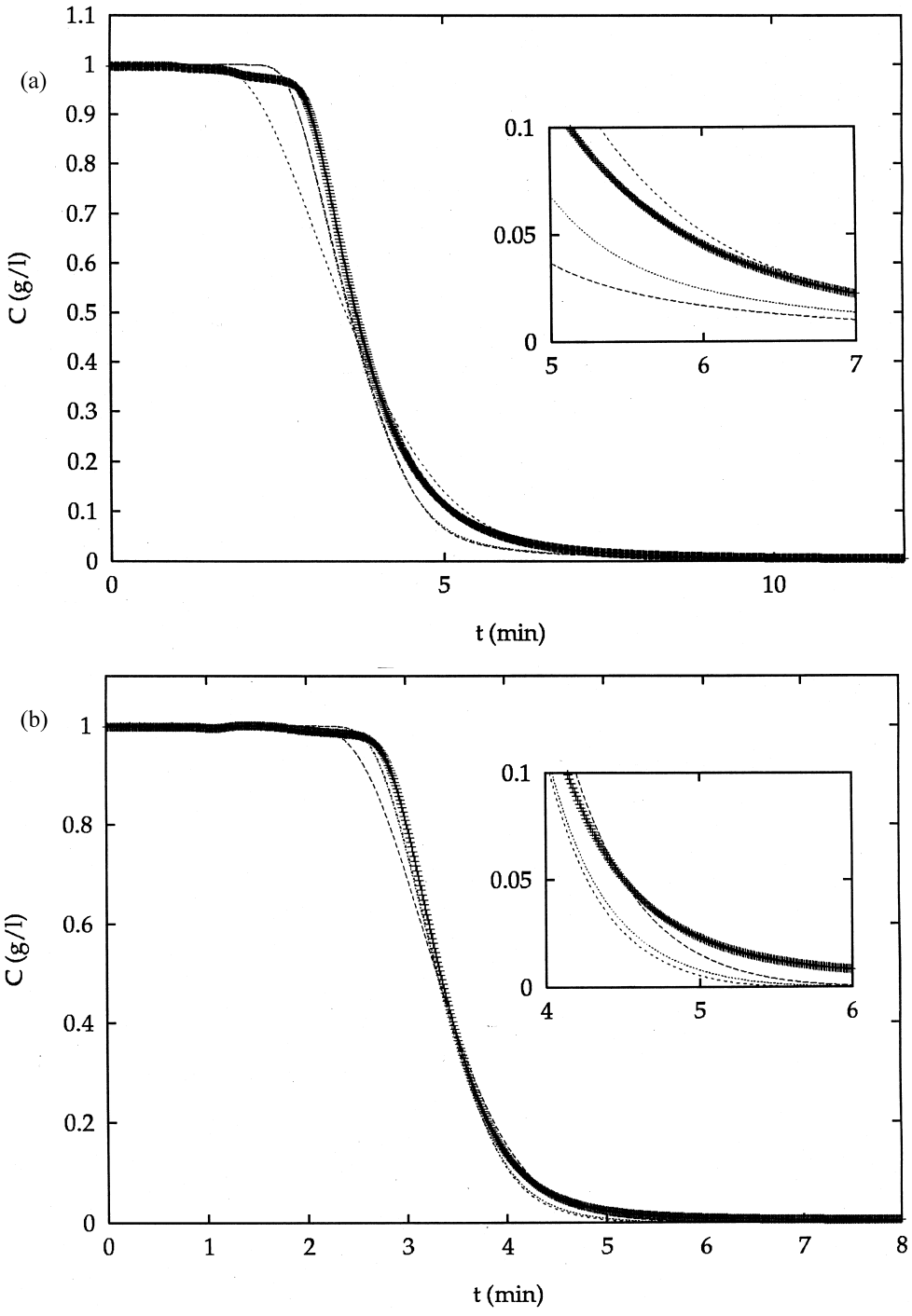

Fig. 8. Illustration of the effect of the concentration dependence of k_f on the shape of a breakthrough curve (symbols). Concentration step from $C_n=1$ to $C_{n+1}=0$ g/l. (a) L-PA. Numerical calculations (lines): $k_f=10$ min^{-1} (short dashed lines), $k_f=110$ min^{-1} (long dashed lines) and $k_f=117.3C^{0.2582}$ min^{-1} (dotted lines). (b) D-PA. Numerical calculations (lines): $k_f=35$ min^{-1} (short dashed lines), $k_f=90$ min^{-1} (long dashed lines) and $k_f=90.9C^{0.1147}$ min^{-1} (dotted lines).

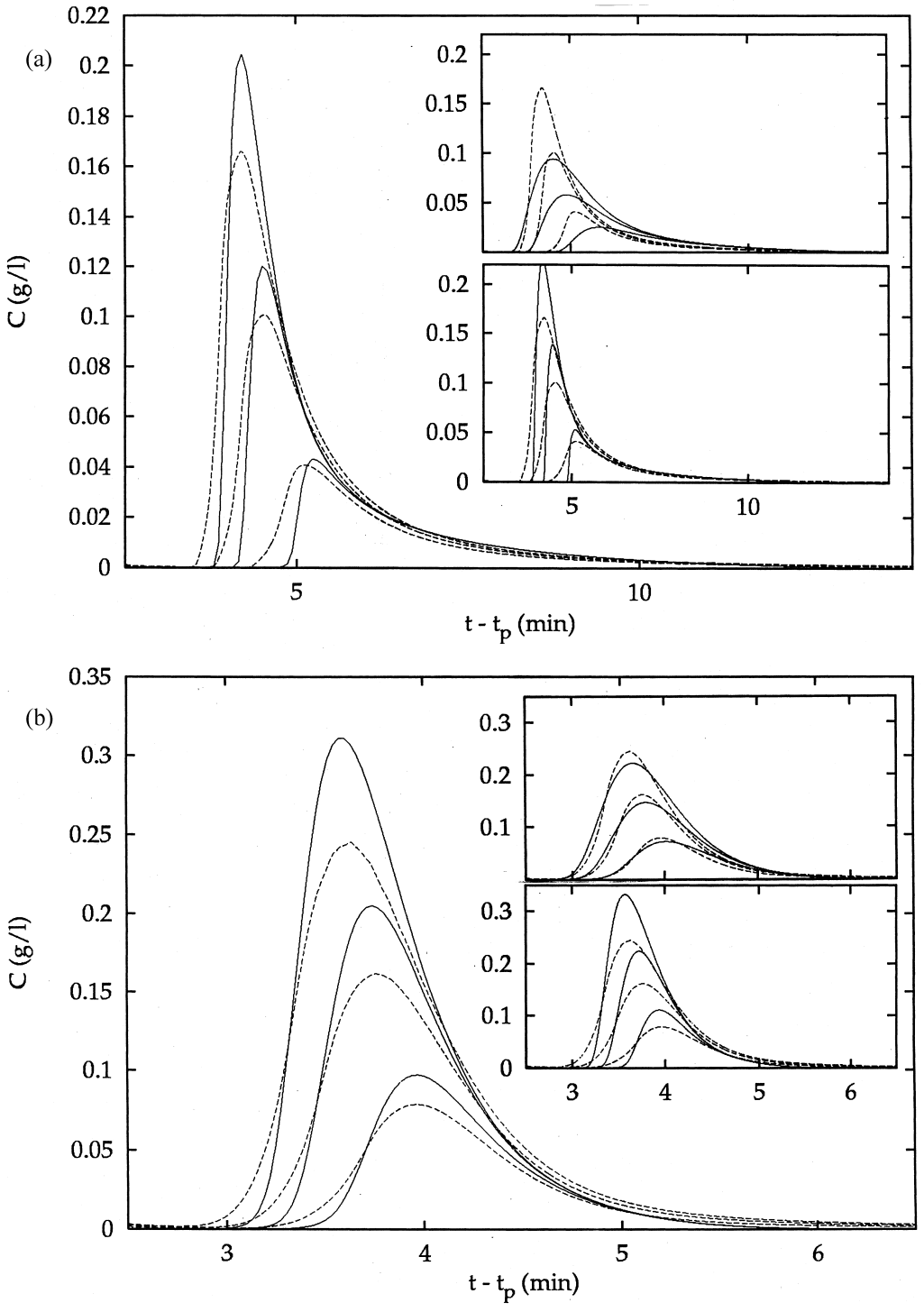

Fig. 9. Example of overloaded elution profiles. Sample volumes: 240, 160 and 80 μl. Sample concentration: 1 g/l. Temperature: 40°C. Experimental data: dotted lines. Numerical calculations: solid lines. (a) L-PA, main figure: $k_f = 117.3C^{0.2582}$ min^{-1}, upper inset: $k_f = 10$ min^{-1}, lower inset: $k_f = 110$ min^{-1}. (b) D-PA, main figure: $k_f = 90.9C^{0.1147}$ min^{-1}, upper inset: $k_f = 35$ min^{-1}, lower inset: $k_f = 90$ min^{-1}.

use in analytical applications, the physical and chemical factors or reactions which affect the site distribution and the mass transfer kinetics need to be identified. Such information should be obtained by carrying out similar determinations using L-PA selective materials with different pore structures or which have been subjected to various chemical or physical modifications [25].

Acknowledgements

This work has been supported in part by grant CHE-9701680 from the National Science Foundation and by the cooperative agreement between the University of Tennessee and Oak Ridge Laboratory. We acknowledge the support of Maureen S. Smith and Torgny Fornstedt in solving our computational problems.

References

[1] G. Wulff, Angew. Chem. Int. Ed. Engl. 34 (1995) 1812.
[2] K.J. Shea, Trends Polym. Sci. 2 (1994) 166.
[3] K. Mosbach, Trends Biochem. Sci. 19 (1994) 9.
[4] B. Sellergren, Trends Anal. Chem. 16 (1997) 310.
[5] A.G. Mayes, K. Mosbach, Trends Anal. Chem. 16 (1997) 321.
[6] B. Sellergren, in: G. Subramanian (Ed.), A Practical Approach to Chiral Separations by Liquid Chromatography, VCH, Weinheim, 1994, p. 69.
[7] B. Sellergren, K.J. Shea, J. Chromatogr. A 690 (1995) 29.
[8] K.J. Shea, D. Spivak, B. Sellergren, J. Am. Chem. Soc. 115 (1993) 3368.
[9] G. Vlatakis, L.I. Andersson, R. Müller, K. Mosbach, Nature 361 (1993) 645.
[10] L.I. Andersson, R. Müller, G. Vlatakis, K. Mosbach, Proc. Natl. Acad. Sci. 92 (1995) 4788.
[11] L.I. Andersson, Anal. Chem. 68 (1996) 111.
[12] B. Sellergren, M. Lepistö, K. Mosbach, J. Am. Chem. Soc. 110 (1988) 5853.
[13] G. Guiochon, S. Golshan-Shirazi, A. Katti, Fundamentals of Preparative and Nonlinear Chromatography, Academic Press, New York, 1994.
[14] H. Guan-Sajonz, P. Sajonz, G. Zhong, G. Guiochon, Biotechnol. Progr. 12 (1996) 380.
[15] P. Sajonz, H. Guan-Sajonz, G. Zhong, G. Guiochon, Biotechnol. Progr. 13 (1997) 170.
[16] A. Seidel-Morgenstern, S.C. Jacobson, G. Guiochon, J. Chromatogr. 637 (1993) 19.
[17] M. Friedrich, A. Seidel, D. Gelbin, Chem. Eng. Process 24 (1988) 33.
[18] W. Gallagher, C. Woodward, Biopolymers 26 (1989) 2001.
[19] K. Lederer, I. Amtmann, S. Vijaykumar, J. Billiani, J. Liq. Chromatogr. 13 (1990) 1849.
[20] S. Gibbs, A. Chu, E. Lightfoot, T. Root, J. Phys. Chem. 95 (1991) 467.
[21] D. Leaist, L. Hao, J. Chem. Soc., Faraday Trans. 89 (1993) 2775.
[22] B. Al-Duri, G. McKay, J. Chem. Tech. Biotechnol. 55 (1992) 245.
[23] P. Sajonz, G. Zhong, G. Guiochon, J. Chromatogr. A 728 (1996) 15.
[24] P. Sajonz, G. Zhong, G. Guiochon, J. Chromatogr. A 731 (1996) 1.
[25] B. Sellergren, K.J. Shea, J. Chromatogr. 635 (1993) 31.
[26] M. Lepistö, B. Sellergren, J. Org. Chem. 54 (1989) 6010.
[27] B. Sellergren, Macromol. Chem. 190 (1989) 2703.
[28] S. Golshan-Shirazi, G. Guiochon, J. Chromatogr. 603 (1992) 1.
[29] M. Jaroniec, R. Madey, Physical Adsorption on Heterogeneous Solids, Elsevier, Amsterdam, 1988.